The EMBO Journal Vol.17 No.24 pp.7179–7189, 1998

FRET microscopy demonstrates molecular association of non-specific lipid transfer protein (nsL-TP) with fatty acid oxidation enzymes in peroxisomes

Fred S.Wouters[1,2,3], Philippe I.H.Bastiaens[2,3], Karel W.A.Wirtz[1] and Thomas M.Jovin[2,4]

[1]Centre for Biomembranes and Lipid Enzymology, Institute of Biomembranes, Utrecht University, Padualaan 8, NL-3584 CH, Utrecht, The Netherlands and [2]Department of Molecular Biology, Max Planck Institute for Biophysical Chemistry, Am Fassberg 11, D-37077, Göttingen, Germany

[3]Present address: Cell Biophysics Laboratory, Imperial Cancer Research Fund, P.O. Box 123, Lincoln's Inn Fields, London WC2A 3PX, UK

[4]Corresponding author
e-mail: tjovin@mpc186.mpibpc.gwdg.de

The fate of fluorescently labeled pre-nsL-TP (Cy3-pre-nsL-TP) microinjected into BALB/c 3T3 fibroblasts was investigated by confocal laser scanning microscopy. The protein exhibited a distinct punctate fluorescence pattern and colocalized to a high degree with the immunofluorescence pattern for the peroxisomal enzyme acyl-CoA oxidase. Proteolytic removal of the C-terminal leucine of the putative peroxisomal targeting sequence (AKL) resulted in a diffuse cytosolic fluorescence. These results indicate that microinjected Cy3-pre-nsL-TP is targeted to peroxisomes. The association of nsL-TP with peroxisomal enzymes was investigated in cells by measuring fluorescence resonance energy transfer (FRET) between the microinjected Cy3-pre-nsL-TP and Cy5-labeled antibodies against the peroxisomal enzymes acyl-CoA oxidase, 3-ketoacyl-CoA thiolase, bifunctional enzyme, PMP70 and catalase. The technique of photobleaching digital imaging microscopy (pbDIM), used to quantitate the FRET efficiency on a pixel-by-pixel basis, revealed a specific association of nsL-TP with acyl-CoA oxidase, 3-ketoacyl-CoA thiolase and bifunctional enzyme in the peroxisomes. These observations were corroborated by subjecting a peroxisomal matrix protein fraction to affinity chromatography on Sepharose-immobilized pre-nsL-TP. Acyl-CoA oxidase was retained. These studies provide strong evidence for a role of nsL-TP in the regulation of peroxisomal fatty acid β-oxidation, e.g. by facilitating the presentation of substrates and/or stabilization of the enzymes.

Keywords: acyl-CoA oxidase/fluorescence resonance energy transfer/3-ketoacyl-CoA thiolase/ PMP70/sterol carrier protein-2

Introduction

The non-specific lipid transfer protein (nsL-TP, also called sterol carrier protein 2, SCP_2) is a basic (pI 8.5–9) protein of 14 kDa which catalyzes the transfer *in vitro* of glycerophospholipids, glycolipids and sterols (Bloj and Zilversmit, 1977, 1981; Crain and Zilversmit, 1980; Chanderbhan *et al*., 1982; Gadella and Wirtz, 1991). By virtue of this transfer activity, nsL-TP stimulates a number of enzyme activities related to cholesterol metabolism (Billheimer and Reinhart, 1990; Ossendorp *et al*., 1994). nsL-TP is synthesized on cytoplasmic polyribosomes as a 15 kDa protein containing a 20-amino-acid pre-sequence (Trzeciak *et al*., 1987; Fujiki *et al*., 1989) and a C-terminal tripeptide Ala-Lys-Leu. This tripeptide corresponds to the PTS1 consensus sequence (Ser/Ala/Cys)-(Lys/Arg/His)-Leu for peroxisomal targeting (Gould *et al*., 1987, 1989, 1990) and accounts for the peroxisomal localization of nsL-TP established by various immunocytochemical and biochemical techniques (Van der Krift *et al*., 1985; Tsuneoka *et al*., 1988; Keller *et al.,* 1989). The function of the presequence remains unknown, but it has been presumed to be involved in mitochondrial targeting (Keller *et al*., 1989; Billheimer *et al*., 1990; Moncecchi *et al*., 1991). After synthesis in the cytoplasm, pre-nsL-TP is imported into the peroxisomes via a receptor-mediated process (reviewed by Subramani, 1998) and converted into nsL-TP by cleavage of the presequence (Fujiki *et al*., 1989; Suzuki *et al*., 1990).

The *in vivo* function of nsL-TP has been a matter of extensive research and contention. The predominantly peroxisomal localization seems to exclude a role in intracellular lipid transport. This conclusion is supported by the lack of an involvement of nsL-TP in the intracellular trafficking of lysosomal cholesterol (Johnson and Reinhart, 1994). Moreover, there does not seem to be any clear correlation between intracellular levels of nsL-TP and the metabolism of cholesterol *in situ* (Van Heusden *et al*., 1985, 1992; Geelen *et al*., 1987). In contrast, there are various indications for a role of nsL-TP in peroxisomal fatty acid β-oxidation. The 58 kDa protein (also called SCPx) containing the complete sequence of pre-nsL-TP at the C-terminus is 50% homologous to peroxisomal 3-ketoacyl-CoA thiolase (Ossendorp *et al*., 1991; Seedorf and Assmann, 1991). Recently, it has been shown that SCPx possesses a 3-ketoacyl-CoA thiolase activity operating on medium-chain fatty acids (octanoyl-CoA) (Seedorf *et al*., 1994) and, in contrast to the peroxisomal Type I thiolase, branched chain intermediates (Antonenkov *et al.*, 1997; Wanders *et al.*, 1997). It has been suggested that the presence of 3-ketoacyl-CoA thiolase and lipid transfer activity in a single protein results from gene fusion (Baker *et al*., 1991) and may denote an interdependence of the two activities. Disruption of the nsL-TP gene encoding both nsL-TP and SCPx leads to a severe deficiency of the peroxisomal β-oxidation of pristanic acid in mice (Seedorf *et al.*, 1998). The yeast analog of nsL-TP, PXP18, is expressed in peroxisomes provided the cells are grown on oleic acid (Tan *et al*., 1994). Recently, Niki *et al.* (1994) demonstrated an interaction of PXP18 *in vitro* with yeast

peroxisomal acyl-CoA oxidase. PXP18 protected acyl-CoA oxidase against heat-induced denaturation, suggesting that PXP18 might function as a molecular chaperone maintaining the integrity of peroxisomal proteins.

In the present study, we assessed the peroxisomal import of microinjected fluorescently labeled rat liver pre-nsL-TP (Cy3-pre-nsL-TP) by confocal laser scanning microscopy (CLSM) in the living cell. Proteolytic removal of the C-terminal leucine established the functionality of the putative peroxisomal targeting. The association of Cy3-nsL-TP imported into the peroxisomes with enzymes of the fatty acid β-oxidation pathway was determined by fluorescence resonance energy transfer (FRET) between Cy3-nsL-TP and Cy5-labeled antibodies raised against the various enzymes. These interactions were investigated in parallel by affinity chromatography of peroxisomal matrix proteins on columns of Sepharose-bound pre-nsL-TP.

Results

Fluorescent labeling and characterization

Purified pre-nsL-TP was labeled with the sulfoindocyanine dye Cy3 and the various antibodies to peroxisomal enzymes were labeled with Cy5. Under the conditions of labeling, a Cy3:pre-nsL-TP molar ratio of 0.7 and Cy5:antibody molar ratios of 5–7.5 were obtained. Cy3-pre-nsL-TP was incubated with a rat liver M-fraction to remove the pre-sequence by proteolysis (Ossendorp *et al*., 1992). As a result of this treatment, the molecular mass of Cy3-pre-nsL-TP shifted from 15 kDa (Figure 1, lane 1) to 14 kDa (Figure 1, lane 2), a position corresponding to nsL-TP. Transillumination with UV demonstrated that the Cy3 fluorescence was restricted to pre-nsL-TP and nsL-TP (Figure 1, lanes 3 and 4). In the latter case, no fluorescence was observed in the front, indicating that free dye was absent and the pre-sequence was unlabeled.

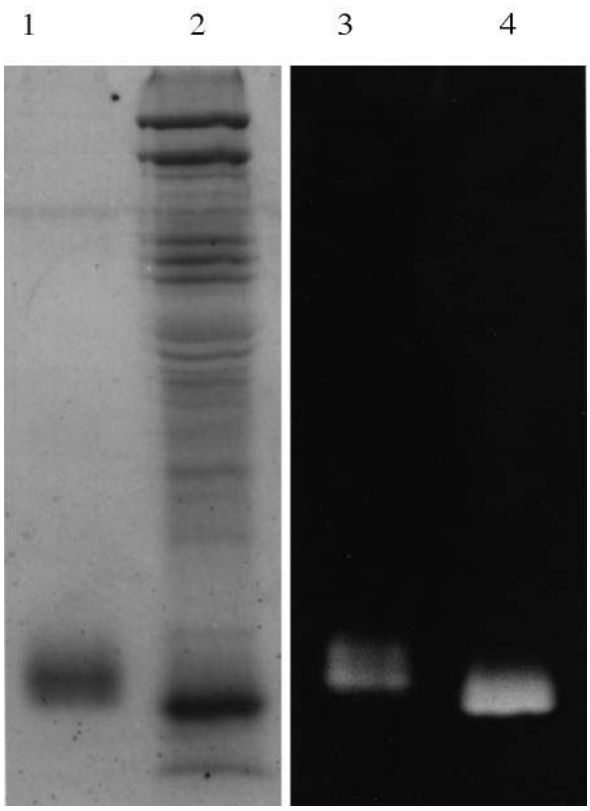

Fig. 1. Characterization of Cy3-pre-nsL-TP. Total protein staining with Coomassie Brilliant Blue (lanes 1–2) and UV transillumination Cy3 fluorescence (lanes 3–4). Lane 1, Cy3 labeled rat liver pre-nsL-TP (1 μg); lane 2, Cy3 labeled rat liver pre-nsL-TP (10 μg) incubated with rat liver M-fraction (75 μg) as described in Materials and methods; lane 3, fluorograph of lane 1; lane 4, fluorograph of lane 2.

Targeting of Cy3-pre-nsL-TP to peroxisomes

After microinjection of Cy3-pre-nsL-TP in BALB/c 3T3 cells, CLSM images revealed a punctate fluorescence pattern distributed throughout the cytoplasm and indicative of peroxisomes (Figure 2A). Upon import of pre-nsL-TP in peroxisomes the presequence is removed; processing is substantial at 17 min and complete within 45 min (Fujiki *et al*., 1989; Suzuki *et al*., 1990). Since the Cy3 probe was located on the mature part of the protein (Figure 1), we infer that the fluorescence signals associated with peroxisomes corresponded to processed Cy3-nsL-TP.

The peroxisomal localization of the microinjected Cy3-labeled pre-nsL-TP was further confirmed by digestion with carboxypeptidase A to remove leucine from the C-terminal alanine-lysine-leucine (AKL), the putative peroxisomal targeting sequence. Digestion of unlabeled pre-nsL-TP under these conditions was assessed by determination of the molecular mass using electrospray mass spectrometry (Figure 3).The peak shifted from 15 166 mass units for pre-nsL-TP (Figure 3A) to 15 053 mass units for the treated protein (Figure 3B), indicating that the digestion was complete and specific for the C-terminal leucine. Upon microinjection, the truncated Cy3-pre-nsL-TP exhibited a diffuse labeling in the cell (Figure 2B), attesting to the essential role of the C-terminal AKL sequence in pre-nsL-TP as a peroxisomal targeting signal. The Cy3 fluorescence in the punctate structures was also unambiguously assigned to peroxisomes by colocalization with the immunofluorescence patterns of the peroxisomal marker protein acyl-CoA oxidase (Figure 2C and D). The Cy3 fluorescence observed in the nucleus reflects unimported pre-nsL-TP. In order to estimate the amount of microinjected protein relative to endogenous nsL-TP, the immunofluorescence intensities of Cy5-labeled anti-nsL-TP antibodies (Cy5-8602) were compared in injected and control cells on the same coverslip. The amount of microinjected protein was ~1.6 ± 0.9 times that of the endogenous nsL-TP.

FRET by pbDIM

The complexation of nsL-TP with peroxisomal fatty acid oxidation enzymes was assessed by *in situ* FRET experiments. After microinjection of Cy3-pre-nsL-TP, cells were fixed and incubated with Cy5-labeled antibodies directed against the following peroxisomal enzymes: acyl-CoA oxidase, bifunctional enzyme, 3-ketoacyl-CoA thiolase, catalase and PMP70, the first three of which are involved in β-oxidation of fatty acids. The range over which FRET between a donor (Cy3) and an acceptor (Cy5) fluorescent molecule varies in a sensitive manner is dictated by the spectral parameter R_o, i.e. the distance at which the FRET efficiency is 50%. R_o for the Cy3–Cy5 system is 5 nm (Bastiaens and Jovin, 1996, 1998). Due to the sixth-power dependency on distance, the FRET efficiency with this

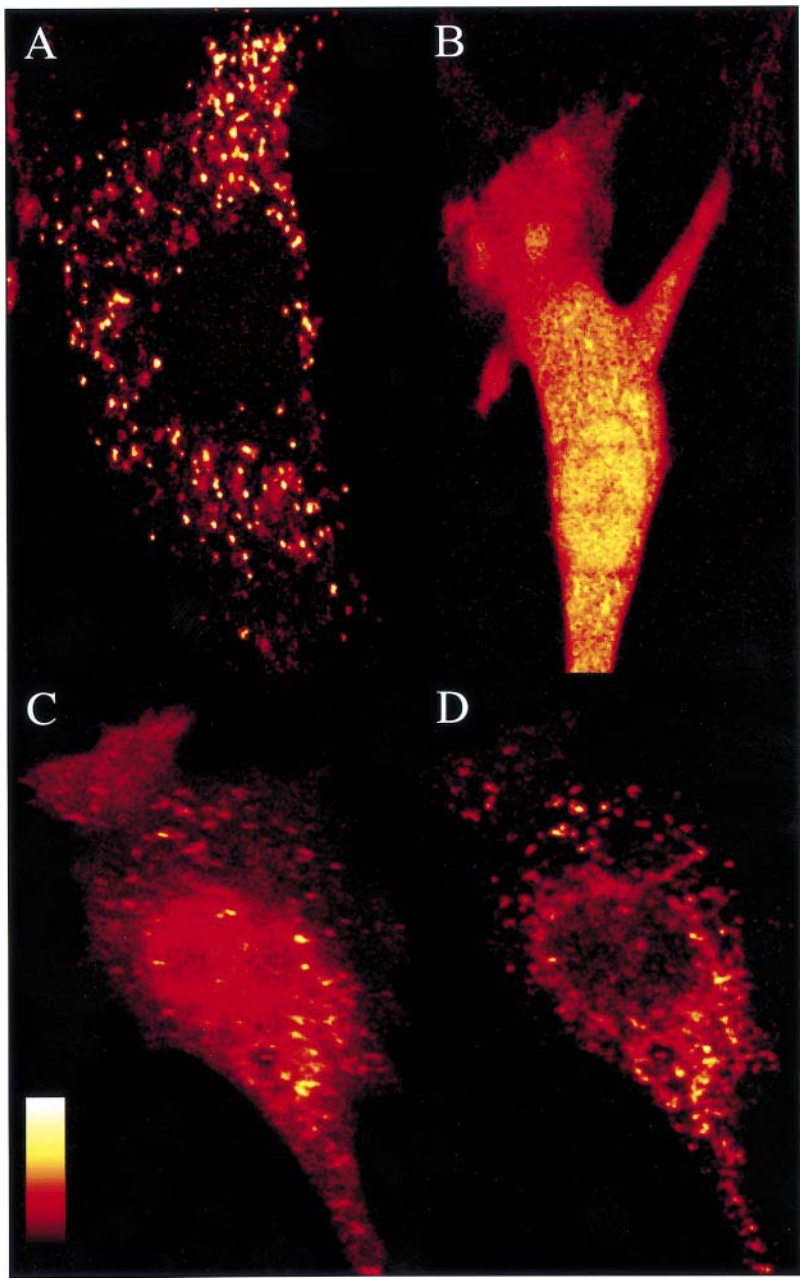

Fig. 2. Peroxisomal import of Cy3-pre-nsL-TP. After microinjection into BALB/c 3T3 cells, (**A**) Cy3-pre-nsL-TP and (**B**) Cy3-pre-nsL-TP lacking the C-terminal leucine were examined by CSLM in living cells. Colocalization between (**C**) microinjected Cy3-pre-nsL-TP and (**D**) Cy5-labeled antibody against acyl-CoA oxidase in fixed cells. Color bar: intensities are represented in black (low) to white (high).

donor–acceptor pair is $<10\%$ beyond 7.2 nm. The rationale of the experiments was that FRET between Cy3-nsL-TP and a Cy5-labeled antibody would occur with detectable efficiency only for those cases in which intimate interactions between the respective proteins were present.

The first enzyme tested by FRET for its association with Cy3-nsL-TP was acyl-CoA oxidase using the combined approach of acceptor and donor pbDIM (Bastiaens *et al*., 1996; Bastiaens and Jovin, 1998; see Materials and methods). Cells microinjected with Cy3-pre-nsL-TP were incubated with Cy5-anti-acyl-CoA oxidase antibodies, and the corresponding FRET efficiencies determined by the CLSM acceptor photobleaching technique (Figure 4A). The first acquired image (D1) is the fluorescence intensity distribution of the donor Cy3-nsL-TP directly excited at 543 nm. The second image (A1) represents the fluorescence intensity distribution of the acceptor Cy5-anti-acyl-CoA oxidase excited at 633 nm. The acceptor fluorophore was subsequently photobleached in part of the field (demarcated by a white rectangle in A2) by repeated scanning with the 633 nm laser line, thereby abolishing FRET. A second donor fluorescence image (D2) was obtained with 543 nm excitation. An increase of donor fluorescence intensity would be expected in the region of acceptor photobleaching only in those cellular structures exhibiting FRET. This effect was apparent exclusively in the peroxisomal punctate structures containing Cy3-nsL-TP (Figure 4B, donor difference image D2–D1), indicating the existence of a complex between nsL-TP and acyl-CoA oxidase in peroxisomes. The FRET efficiency throughout

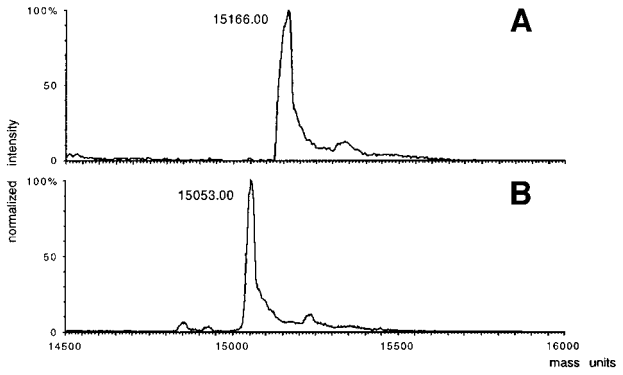

Fig. 3. Electron spray mass spectrographs of carboxypeptidase A-treated pre-nsL-TP. (**A**) Purified recombinant rat liver pre-nsL-TP. (**B**) Carboxypeptidase A-treated pre-nsL-TP. The indicated mass units are identical to the calculated mass units.

the cell was calculated by a simple image arithmetic operation (Figure 4B, [D2–D1]/D2). As expected, the FRET efficiency outside the white rectangle (Figure 4B, upper panel) was near zero.

A second independent assessment of FRET in the cells was made from the donor photobleaching kinetics (Figure 4C). The part of the cell in which the acceptor was photodestroyed (Figure 4D, white rectangle) and thus FRET was abolished served as the reference. The average donor photobleaching time (τ_r) in the reference region was used to calculate FRET elsewhere in the image. That is, the donor photobleaching time increased at sites where FRET was operative (Bastiaens and Jovin, 1996). This effect is seen in Figure 4D, which depicts the computed time constants τ for every pixel in pseudocolor. Noteworthy are the longer τ values indicative of FRET in punctate structures outside the reference region. The τ values for the non-imported Cy3-nsL-TP, observed as a diffuse staining in the cytoplasm and nucleus, were comparable to those within the reference region, demonstrating that FRET was only evident for Cy3-nsL-TP imported into peroxisomes.

The FRET efficiency was calculated for every pixel outside the reference region according to Equation 2 (Materials and methods; Figure 4E). The highest efficiencies were restricted to punctate structures. The specificity of the phenomenon was evident from the saturation of the FRET efficiency with increasing amounts of Cy5-labeled antibody (Figure 4E). At the highest dilutions (3200- and 1600-fold) no FRET was evident, while at a dilution of 600-fold, the FRET efficiency was substantial, ~30%, a value which did not increase further at still lower dilutions (higher concentrations). This finding confirmed that the observed complexes were specific, as was also apparent from the relative distribution of τ values (and the corresponding FRET efficiencies), within and outside the reference regions. Based on these results, the 600-fold dilution was used in all further experiments. The concentrations of the other antibodies were adjusted so as to obtain Cy5-fluorescence intensities equivalent to that of the 600-fold diluted anti-acyl-CoA oxidase.

The same technique was used to investigate possible associations of the other peroxisomal proteins to nsL-TP (Figure 5). Column 1 depicts the donor (Cy3-nsL-TP) fluorescence intensity distribution in the cells, and column 2 the corresponding acceptor (Cy5-labeled antibody) signal; the white rectangle denotes the location of the acceptor-free region after Cy5 photodestruction. The FRET efficiencies were calculated from the acceptor photobleaching method by division of the donor fluorescence intensity images before and after Cy5 photodestruction (Equation 1, Materials and methods; Figure 5, column 3) and by analyzing the donor photobleaching kinetics (Figure 5, column 4). FRET was restricted to punctate structures and was substantial with antibodies raised against bifunctional enzyme, 3-ketoacyl-CoA thiolase and PMP70, but negligible with the antibodies against catalase (Figure 5, row 4), the values for which were comparable to those in the absence of antibody. From these observations we conclude that acyl-CoA oxidase, 3-ketoacyl-CoA thiolase, bifunctional enzyme and PMP70 are in close molecular proximity to nsL-TP, but not to catalase. The structures exhibiting FRET matched the peroxisomal staining by Cy3-nsL-TP. That is, the extraperoxisomal Cy3-pre-nsL-TP did not produce a finite FRET signal, as already noted above.

Statistical evaluations were made of the FRET data in the various confocal images (Table I; Materials and methods). The mean ± SD estimations from the donor and acceptor photobleaching experiments on regions from single cells were consistent (within experimental error). The combined mean FRET efficiencies for the various peroxisomal target proteins increased in the order: catalase $\approx 0 <$ bifunctional enzyme (0.13) $<$ PMP70 (0.24) $\approx$ acyl-CoA oxidase (0.24) $<$ 3-ketoacyl-CoA thiolase (0.33). The projected area/peroxisome was quite similar for all the target proteins.

During fluorescent detection of microinjected and endogenous nsL-TP and peroxisomal marker enzymes it was observed that nsL-TP and the marker enzymes did not invariably display the same pattern. nsL-TP was always detected in globular peroxisomes in both live and fixed cells, whereas the marker enzymes were also detected in elongated peroxisomes (Figure 5, columns 1 and 2). Such a heterogeneity in morphology and protein composition has been reported previously (Schrader *et al*., 1995, 1996; Wilcke *et al.*, 1995).

Affinity chromatography of peroxisomal matrix proteins

The complexation of peroxisomal β-oxidation enzymes with nsL-TP was further investigated by affinity chromatography of rat liver peroxisomal matrix proteins on a pre-nsL-TP–Sepharose column. As a control for nonspecific binding, the matrix proteins were also applied to bovine serum albumin (BSA)- and lysozyme–Sepharose columns. Lysozyme was selected because the protein is small and basic, like nsL-TP.

Under high salt conditions (120 mM KCl), acyl-CoA oxidase eluted from the nsL-TP column in two peaks (Figure 6A). The immunoreactive bands at 71 and 52 kDa corresponded to the A and B subunits of acyl-CoA oxidase, respectively (Osumi *et al*., 1980). The first peak (fractions 3–12) was recovered in the run-through. The second peak (fractions 17–26) was retained on the column, showing an interaction of acyl-CoA oxidase with nsL-TP. The biphasic elution pattern was also observed when smaller amounts of matrix proteins were applied to the column,

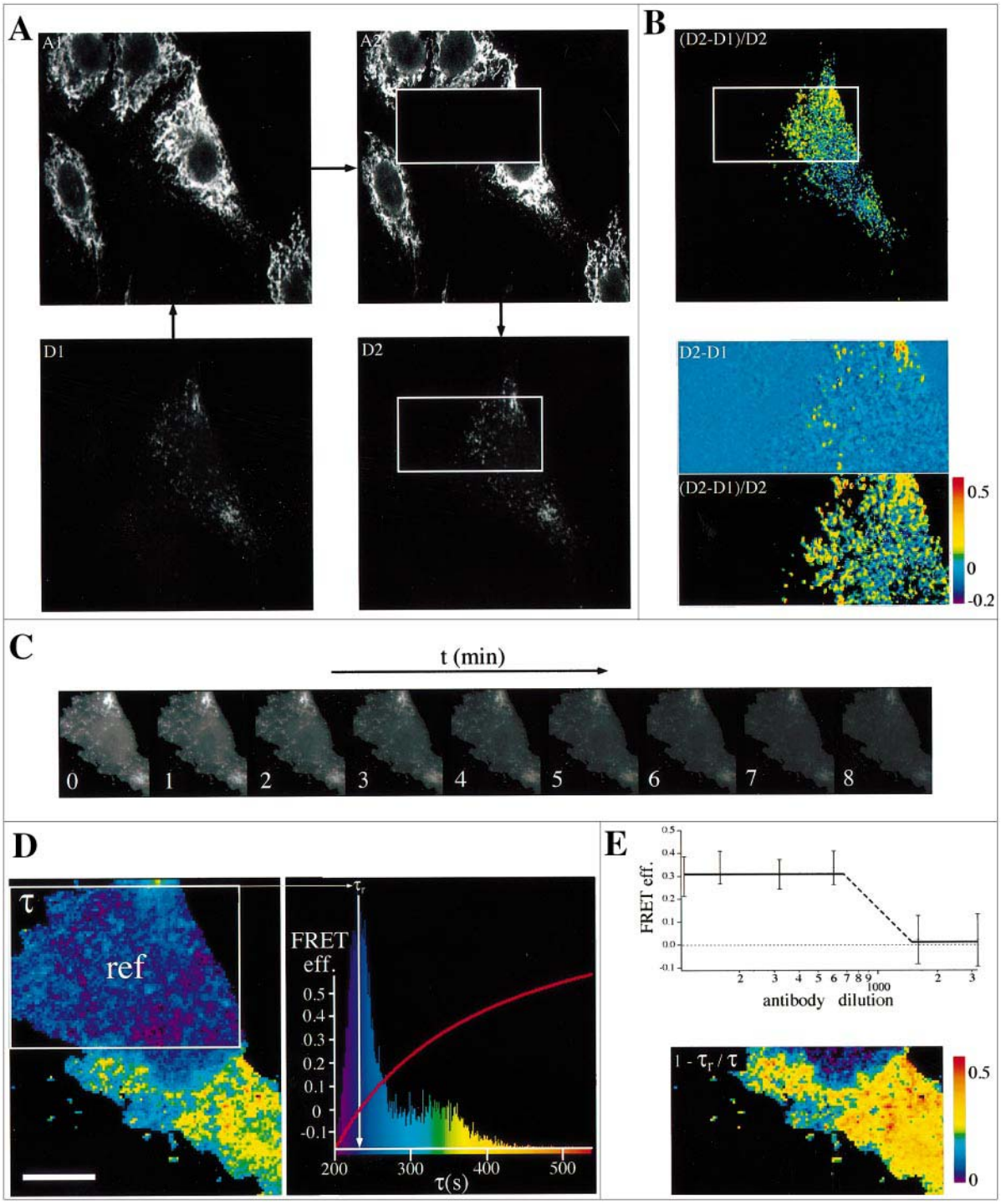

Fig. 4. Interaction between nsL-TP and acyl-CoA oxidase monitored by FRET between Cy3-nsL-TP and Cy5-labeled anti-acyl-CoA oxidase antibodies. Cy3-pre-nsL-TP microinjected BALB/c 3T3 fibroblasts were incubated with Cy5-labeled α-acyl-CoA oxidase antibodies. (**A**) Sequence of events to obtain FRET efficiency maps from acceptor photobleaching. A donor image D1 (Cy3-nsL-TP fluorescence intensity image) and acceptor image A1 (Cy5-labeled α-acyl-CoA oxidase fluorescence intensity image) are acquired. The acceptor is photobleached in a specific portion of the cell by continuous scanning with the 633 nm laser line (A2). The intracellular reference regions created by Cy5 photodestruction are enclosed in white rectangles. After photodestruction of Cy5 a second donor image D2 is obtained. (**B**) Calculated FRET efficiency maps ([D2–D1]/D2) and difference image (D2–D1). The upper image shows the FRET efficiency calculated for the whole field, and the lower image an enlarged area of the difference image (top half) and FRET efficiency (bottom half) where Cy5 was photobleached. (**C**) First nine images of a donor photobleaching series with the same cell as in (A). (**D**) Calculated photobleaching time map (τ) and photobleaching time histogram with the reference region in which the acceptor Cy5 was photodestructed marked by a white rectangle (ref), and reference photobleaching time (τ_r) marked by a white arrow. The red curve in the histogram provides the mapping from τ values to FRET efficiencies. Bar: 10 μm. (**E**) Lower panel, FRET efficiency map outside reference region calculated from donor photobleaching kinetics; upper panel, average FRET efficiency in peroxisomes as a function of Cy5-labeled α-acyl-CoA oxidase antibody dilution.

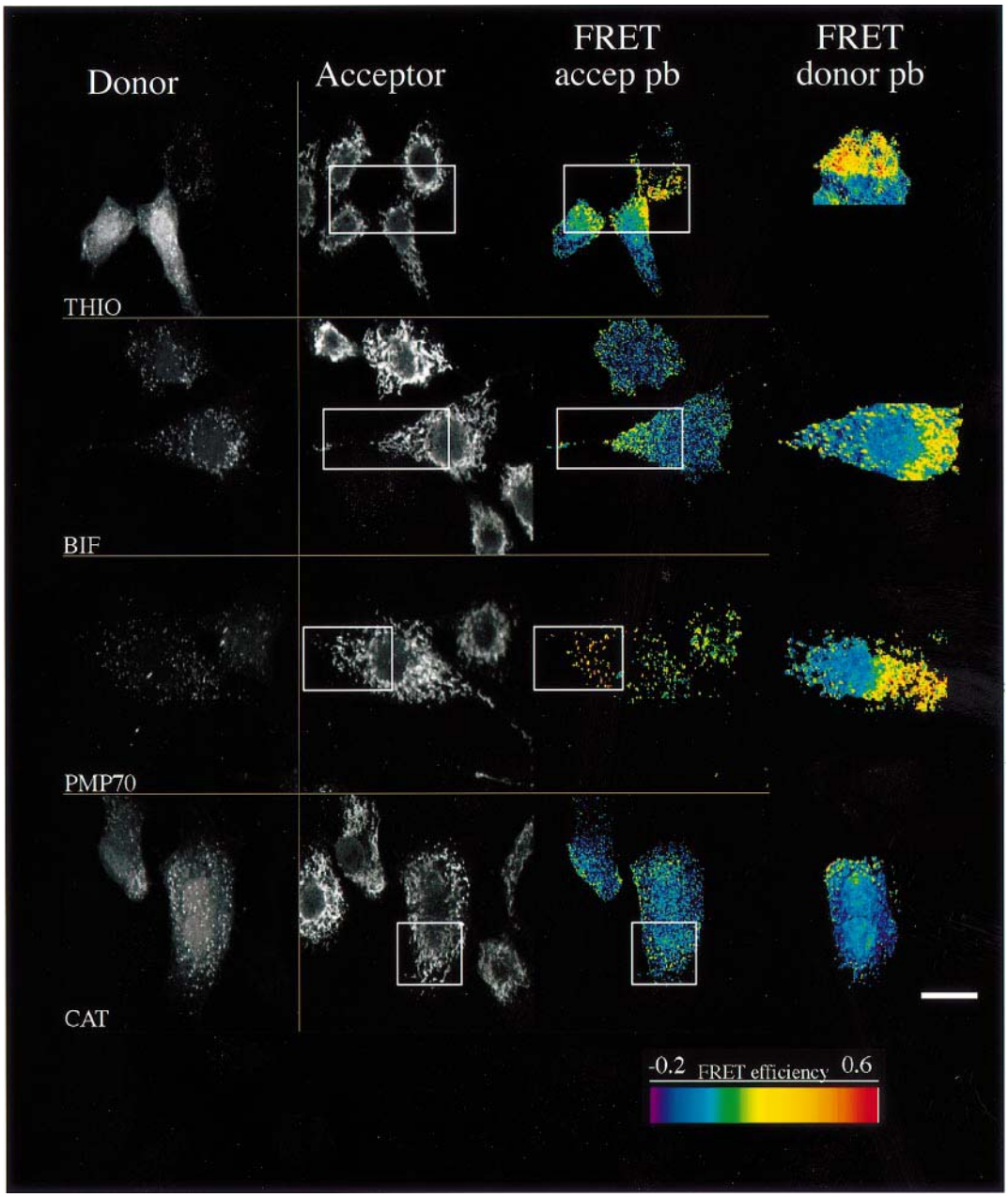

Fig. 5. Detection of molecular interaction between Cy3-nsL-TP and peroxisomal proteins by acceptor/donor photobleaching FRET microscopy. BALB/c 3T3 mouse fibroblasts were microinjected with Cy3-pre-nsL-TP and counterstained with Cy5-labeled antibodies directed against peroxisomal enzymes. Vertical columns from left to right: column 1, fluorescence of microinjected Cy3-nsL-TP (donor); column 2, fluorescence of Cy5-labeled antibody against peroxisomal protein (acceptor). The region in which the acceptor was photobleached is marked by a white rectangle. The following antibodies were tested: 3-ketoacyl-CoA thiolase (THIO), bifunctional enzyme (BIF), peroxisomal membrane protein 70 kDa (PMP70) and catalase (CAT). Column 3, FRET efficiencies calculated from the ratio of the pre- and post-Cy5 photobleaching donor fluorescence images. Column 4, FRET efficiencies calculated from donor photobleaching kinetics. Bar: 10 μm.

indicating that the two pools may have represented different forms of acyl-CoA oxidase. In support of this conclusion, acyl-CoA oxidase present in the run-through was not retained when again applied to the nsL-TP–Sepharose column. The acyl-CoA oxidase bound to neither the lysozyme- nor the BSA–Sepharose control columns (Figure 6B and C). A further finding was that 3-ketoacyl-CoA thiolase (Figure 6D) and catalase (Figure 6E) were not retained on the nsL-TP–Sepharose column. The affinities of β-oxidation enzymes for nsL-TP were also determined upon application of the peroxisomal matrix proteins to the affinity columns under low salt conditions (25 mM KCl). Acyl-CoA oxidase was quantitatively retained, whereas 3-ketoacyl-CoA thiolase or bifunctional enzyme showed no interaction. Under these low salt conditions, the bulk of acyl-CoA oxidase again exhibited no binding to the lysozyme– or BSA–Sepharose columns.

Discussion

We have demonstrated that the targeting sequence AKL in pre-nsL-TP is active in living BALB/c 3T3 fibroblasts (Figure 2A). Since the protein is synthesized on free polyribosomes in the cytoplasm, we expected that fluores-

Table I. Mean FRET efficiencies in peroxisomes from donor and acceptor photobleaching in single cells

Target protein	Donor photobleaching			Acceptor photobleaching		
	<E>	Eval. area	<area>	<E>	Eval. area	<area>
no Ab	0.02 ± 0.10	2080	4			
CAT	0.00 ± 0.11	3113	22	0.03 ± 0.18	2019	21
BIF	0.19 ± 0.11	1039	27	0.07 ± 0.10	2250	33
PMP70	0.21 ± 0.19	777	11	0.28 ± 0.15	1353	21
AOX	0.26 ± 0.08	1528	27	0.19 ± 0.13	2230	24
THIO	0.32 ± 0.15	1050	18	0.35 ± 0.12	1478	20

Donor, Cy3-pre-nsL-TP; acceptor, Cy5-labeled antibodies to target proteins. <E>, mean ± SD for the FRET signal within the mask; Eval. area, number of pixels used in the evaluation (from ⩾ 1 cell); <area>, area (pixels) per peroxisome. From the mask images, the number of peroxisomes was in the range 70–150. One pixel corresponds to 0.35 μm.

cently labeled pre-nsL-TP (Cy3-pre-nsL-TP) microinjected in the cytoplasm would be likely to follow the same import route as natively expressed protein. This expectation was fulfilled. The destruction of the peroxisomal targeting signal resulted in abolishment of peroxisomal import.

Using a similar approach, it was shown that firefly luciferase containing the C-terminal PTS1 SKL motif and human serum albumin conjugated to a peptide carrying SKL are transported to peroxisomes upon microinjection into BALB/c 3T3 cells (Walton *et al*., 1992). Coinjection of SKL-bearing peptides prevented peroxisomal import of firefly luciferase, demonstrating that the process was saturable. Interestingly, microinjected protein started to appear in peroxisomes 2 h post-injection and reached maximal import at 18 h. This time scale of import was significantly longer than the 30 min which we observed in the case of pre-nsL-TP, for which there was no further increment at longer times. Furthermore, distinct structures were absent after carboxypeptidase treatment of the protein (Figure 2B). We obtained no evidence (in mouse fibroblasts) for a function of the pre-sequence in mitochondrial targeting (Keller *et al*., 1989; Billheimer *et al*., 1990; Moncecchi *et al*., 1991).

There was a punctate distribution of fluorescence intensity in the cells after microinjection of Cy3-pre-nsL-TP (Figure 2A) and after incubation of cells with Cy5-labeled antibodies against nsL-TP, i.e. the endogenous protein (data not shown). Using the Cy5-labeled antibodies against the other peroxisomal enzymes, elongated bodies were observed next to the punctate structures. The existence of a heterogeneous peroxisomal morphology was reported in HepG2 cells fixed with formaldehyde (Schrader *et al*., 1995, 1996), and found to be dependent on the degree of confluency of the cells. In subconfluent cells, peroxisomes were almost exclusively elongated. Although the fibroblasts in our study were maintained subconfluent in order to facilitate microinjection, we never observed elongated peroxisomes containing nsL-TP. Different peroxisomal shapes in primary Leydig cells have been reported using immunofluorescence specific for catalase, acyl-CoA oxidase and 3-keto-acyl-CoA thiolase (Litwin and Bilinska, 1995). Irregular shapes are also present in regenerating rat liver (Yamamoto and Fahimi, 1987).

Using pbDIM, we were able to detect association of nsL-TP and the peroxisomal fatty acid oxidation enzymes acyl-CoA oxidase, 3-ketoacyl-CoA thiolase and bifunctional enzyme (Figures 4 and 5; Table I). The mean values

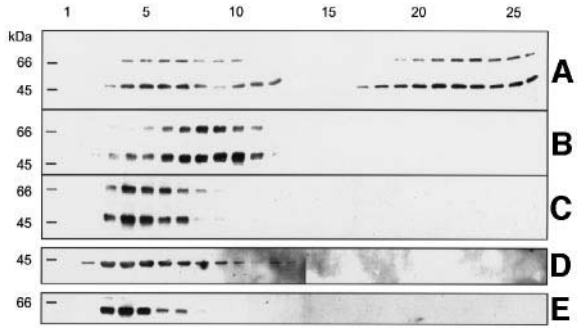

Fig. 6. Affinity chromatography of rat liver peroxisomal matrix fraction on pre-nsL-TP Sepharose: high stringency binding and high stringency elution. Peroxisomal matrix fraction (30 μg of protein) was loaded onto Sepharose 4B columns containing covalently coupled pre-nsL-TP, lysozyme or BSA (7 mg protein/ml resin, 0.7 ml resin) and eluted with high salt buffer. Fractions (0.23 ml) were collected and subjected to Western blotting. Fraction numbers are indicated above the figure, and molecular weight markers are indicated in kDa. Separation of peroxisomal protein on [(**A**), (**D**) and (**E**)] a pre-nsL-TP Sepharose column, (**B**) a lysozyme Sepharose column and (**C**) a BSA Sepharose column. Blots were incubated with [(A), (B) and (C)] anti-acyl-CoA oxidase antibody, (D) anti-thiolase antibody or (E) anti-catalase antibody.

of the FRET efficiencies for the various target proteins were in the range 0.13–0.33. The variations might have reflected: (i) inherent differences in the three-dimensional structure of the individual complexes; (ii) different labeling and binding stoichiometries of the antibodies; and/or (iii) differential accessibilities of the antibodies. We attribute the spread in the FRET efficiency values, indicated by the SD values (Table I), to an actual distribution of values within the peroxisomes and not merely to measurement error. Data analysis based on two-dimensional histograms (not shown) demonstrated no correlation between the FRET values and the fluorescence intensities of the donor or the acceptor, with the exception of PMP70 for which the FRET efficiency increased with acceptor concentration. The latter phenomenon is consistent with the planar distribution of PMP70. On the basis of the FRET and biochemical data we propose that the direct peroxisomal protein partners of nsL-TP are present in the form of a multi-enzyme complex, or alternatively, that nsL-TP forms complexes with the individual enzymes as free species in the peroxisomal matrix. These two options could be addressed by a FRET approach using pairs of specific antibodies or Fabs directed against the individual β-oxidation enzymes labeled with donor/acceptor fluoro-

phores. However, this strategy is disadvantageous due to the anticipated large size of the resultant complex, leading to the separation between donors and acceptors exceeding the critical Förster distance, R_0.

The specific nature of the energy transfer signal was confirmed by the fact that the FRET efficiency was saturable with increasing amounts of Cy5-labeled antibodies. This was checked for the Cy5-acyl-CoA oxidase antibody by donor photobleaching kinetic analysis (Figure 4E). That the observed associations were specific was also apparent from the distribution of τ values within and external to the control region of the FRET experiments.

Unexpectedly, an apparent complexation of PMP70 to nsL-TP was detected using the two independent pbDIM techniques. It is known that nsL-TP can occur in a membrane-bound form (m-nsL-TP) (Van Heusden *et al*., 1990; Van Haren *et al*., 1992), especially in extrahepatic tissues. Thus, a complex with PMP70 might be explained by a membrane-association of Cy3-nsL-TP upon import. On the other hand, we note that PMP70 is the only protein tested that is geometrically restricted within the peroxisome, i.e. is confined to the peroxisomal membrane. The sixth-order dependency of FRET on the separation distance holds for a single donor–acceptor pair. In the case of PMP70, the acceptor is distributed in a plane and the distance dependency of FRET would be reduced to fourth order were this protein to function as an acceptor (Bastiaens *et al*., 1990). Thus, the observed 'association' might reflect this reduced distance dependency and/or the (small) dimensions of the peroxisome. Other proteins known to be localized in the peroxisomal matrix, presumably in a random distribution, should not exhibit this phenomenon.

The identification of an nsL-TP–protein complex inferred from the FRET measurements was confirmed biochemically by nsL-TP-affinity chromatography of a rat liver peroxisomal matrix preparation. Using this technique, specific binding of acyl-CoA oxidase to nsL-TP was detected (Figure 6). However, binding of 3-ketoacyl-CoA thiolase and of bifunctional enzyme to nsL-TP was not demonstrated. The apparent discrepancy between the FRET measurements and the results of affinity chromatography may indicate that 3-ketoacyl-CoA thiolase and bifunctional enzyme bind to nsL-TP indirectly via another protein, possibly acyl-CoA oxidase. The distance between nsL-TP and these enzymes would still fall within the limits of FRET detection, i.e. $\simeq R_0$. Affinity chromatography is not ideally suited for detecting indirect interactions (Phizicky and Fields, 1995). It is conceivable that the particular binding conditions of the affinity chromatography experiments (ionic, concentrations, absence of other factors) were unfavorable for the binding of 3-ketoacyl-CoA thiolase and bifunctional enzyme. In short, negative results in such experiments are not conclusive.

Our findings offer support for the notion that nsL-TP is involved in peroxisomal fatty acid β-oxidation rather than acting as a lipid-transfer (sterol carrier) protein. One can reconcile the earlier observations of lipid-binding exhibiting low affinity and broad specificity with a presumed role in fatty acid oxidation by invoking a shuttle function for nsL-TP. The protein would serve to transport fatty acyl-CoA through the chain of fatty acid oxidizing enzymes, presenting the substrate to the respective active sites and thereby transiently increasing the local concentration. The binding of fatty acyl-CoA to nsL-TP has been reported (Frolov *et al*., 1996). We have also demonstrated the high-affinity binding of CoA esters of very long fatty acids (C24:0, C24:1, C26:0, C26:1) to this protein (unpublished data) and the binding of fatty acid β-oxidation intermediates and branched-chain fatty acyl substrates, with affinities decreasing in the order palmitoyl-CoA > palmitenoyl-CoA >> 3-hydroxypalmitoyl-CoA, 3-oxo-palmitoyl-CoA, phytanoyl-CoA > pristanoyl-CoA (Wouters, 1997). Fast binding kinetics were only observed when the substrates were presented as monomers, i.e. in β-cyclodextrin, corresponding to a function in fatty acid uptake from a β-oxidation enzyme hydrophobic pocket. In the case of SCPx containing the complete sequence of pre-nsL-TP at the C-terminus and shown by Seedorf *et al.* (1994) to contain both a 3-ketoacyl-CoA thiolase activity and lipid transfer activity, the interaction between a lipid-metabolizing enzyme and nsL-TP was achieved physically by a fusion of the two genes. The findings of *in vitro* stimulation of several cholesterol-metabolizing activities by nsL-TP would implicate the low-affinity lipid-binding site in the presentation of the lipid substrate. In a recent report, the yeast analogue of nsL-TP, PXP18, was shown to protect acyl-CoA oxidase against heat-induced denaturation *in vitro* (Niki *et al*., 1994). The authors suggested that nsL-TP might help to stabilize acyl-CoA oxidase and 3-ketoacyl-CoA thiolase, thereby increasing the lifetime of these enzymes. Furthermore, a novel peroxisomal non-specific lipid transfer protein was shown to co-purify with peroxisomal acyl-CoA oxidase in yeast (Ceolotto *et al*., 1996). The finding that nsL-TP is associated with acyl-CoA oxidase, 3-ketoacyl-CoA thiolase and bifunctional enzyme raises the possibility that the β-oxidation enzymes in peroxisomes are organized in a functional complex, leading to an efficient transfer of the lipid intermediates between the enzymes. Functional compartmentalization would seem to be a prevailing principle of intracellular organelles.

Materials and methods

Materials

Recombinant rat pre-nsL-TP was expressed and purified to homogeneity as described in Ossendorp *et al.* (1992). Polyclonal rabbit antisera against rat liver acyl-CoA oxidase, rat liver 3-ketoacyl-CoA thiolase, bovine liver catalase and the C-terminal 26 kDa ABC-binding cassette fragment of recombinant rat liver PMP70 were kindly provided by Prof. Dr H.F.Tabak (Dept of Biochemistry, Academical Medical Centre, Amsterdam, The Netherlands) and against rat liver bifunctional enzyme by Prof. Dr W.W.Just (Institut für Biochemie I, University of Heidelberg, Germany). Monofunctional succinimide esters of sulfoindocyanine fluorescent dyes Cy3.29 OSu (Cy3) and Cy5.29 OSu (Cy5) (Southwick *et al*., 1990) were from Amersham (Buckinghamshire, UK), Microcon and Centricon concentration units from Amicon (Beverly, MA), carboxypeptidase A from Sigma (St Louis, MO) and P10DG Econopac columns and protein assay kit from Bio-Rad (Hercules, CA). Protifar non-fat dried milk powder was from Nutricia (Zoetermeer, The Netherlands), and Protran nitrocellulose (0.45 μm) from Schleicher & Schuell (Dassel, Germany). Horseradish peroxidase conjugated goat-anti-rabbit antibodies (GARPO) were from Nordic Immunology (Tilburg, The Netherlands). Renaissance enhanced chemoluminescence reagents were from Dupont NEN (Boston, MA). CNBr-activated Sepharose 4B was from Pharmacia (Uppsala, Sweden).

Preparation of subcellular fractions

Mitochondrial (M) and light mitochondrial (L) fractions were isolated from a rat liver homogenate by differential centrifugation according to

Völkl and Fahimi (1985). An enriched peroxisomal fraction was prepared by loading the L fraction onto a 30% Nycodenz cushion followed by centrifugation for 45 min at 132 000 *g*. The pellet enriched in peroxisomes was gently resuspended in a buffer consisting of 0.25 M sucrose, 5 mM MOPS–NaOH pH 7.2, 1 mM EDTA and 0.1% ethanol, and stored at –80°C. The matrix proteins (0.17 mg) were isolated from this peroxisomal fraction using the Triton X-114 phase separation method (Bordier, 1981).

Fluorescent labeling of pre-nsL-TP and antibodies

Pre-nsL-TP (4.2 mg/ml) stored at –20°C in 25 mM Tris–HCl pH 7.5, 2.5 mM EDTA, 5 mM 2-mercaptoethanol, 50% glycerol. An aliquot (250 μg) was transferred to labeling buffer [50 mM Bicine–NaOH pH 8.0, 0.5 mM EDTA, 0.5 mM EGTA, 1 mM 2-mercaptoethanol, 120 mM KCl, 10% (v/v) glycerol] by four cycles of concentration and subsequent redilution in a Centricon YM10 concentrator at 4°C up to a final concentration of 1 mg/ml. The labeling reaction was initiated by adding 1 μl of Cy3 reagent in dry DMF (60 mM) to 0.1 ml of pre-nsL-TP (0.1 mg) in labeling buffer. The reaction mixture was incubated for 30 min at room temperature and the reaction was stopped by the addition of glycine (final concentration of 10 mM). The labeled protein was separated from the unconjugated dye by gel permeation chromatography on a P10DG column equilibrated in the buffer used for microinjection [50 mM Tris–HCl pH 7.4, 0.5 mM EDTA, 0.5 mM EGTA, 1 mM 2-mercaptoethanol, 120 mM KCl, 10% (v/v) glycerol].

IgG fractions of polyclonal rabbit antisera were obtained by Protein-G affinity chromatography and were transferred to 0.1 M bicine–NaOH pH 9.0 using a Centricon YM30 concentrator. The IgG fractions were labeled with the Cy5 reagent (10- to 30-fold molar excess) for 30 min at room temperature as described for pre-nsL-TP. Unconjugated dye was removed by chromatography on a P10DG column equilibrated in phosphate-buffered saline (PBS: 137 mM NaCl, 2.7 mM KCl, 8.3 mM Na_2HPO_4, 1.5 mM KH_2PO_4).

Dye to protein molar ratios were determined spectrophotometrically from ε_{554} = 150/mM/cm for Cy3 and ε_{650} = 250/mM/cm for Cy5, and protein concentrations by the Bio-Rad protein assay kit with BSA as standard.

Proteolytic removal of the presequence

The presequence of Cy3-pre-nsL-TP (1 μg) was proteolytically removed by overnight incubation with a rat liver M fraction (75 μg) at 37°C in 0.1 ml 50 mM Tris–HCl pH 7.0, 2 mM EDTA, 10 mM 2-mercaptho-ethanol as described by Ossendorp *et al.* (1992). The cleavage products were identified by applying the total reaction mixture to a 15% SDS–polyacrylamide gel. The gel was transilluminated by UV to detect Cy3 and stained for total protein by Coomassie Brilliant Blue.

Proteolysis of the C-terminus by carboxypeptidase A

Proteolysis of Cy3-pre-nsL-TP by carboxypeptidase A (10 units/μmol) was performed in 6.25 mM Tris–HCl pH 7.4, 0.6 mM EDTA, 12.5% (v/v) glycerol for 30 min at 25°C. Carboxypeptidase A was added from a crystalline stock solution and subsequently removed by filtration on an YM100 concentrator. After the incubation, the treated Cy3-pre-nsL-TP was transferred to the buffer used for microinjection as described in the Fluorescent labeling section.

The extent and specificity of carboxypeptidase A proteolysis was assessed by using unlabeled pre-nsL-TP. The characterization of the product was carried out by Dr W.D.van Dongen (Department of Analytical Molecule Spectrometry, Utrecht University, Utrecht, The Netherlands) using electrospray mass spectrometry.

Microinjection and immunolabeling

Microinjection was carried out on BALB/c 3T3 mouse fibroblasts grown at 37°C on Eppendorf Cellocator coverslips in Dulbecco's modified Eagle's medium (DMEM) supplemented with 10% (v/v) fetal calf serum (FCS) in a 5% CO_2 atmosphere. Prior to microinjection the cells were placed on medium supplemented with 20 mM HEPES–NaOH pH 7.4, and the solution containing Cy3-pre-nsL-TP was centrifuged for 5 min at 100 000 *g* in a Beckman Airfuge. Cells were microinjected using an Eppendorf microinjector equipped with Eppendorf femtotip glass capillaries at an injection pressure of 80 hPa for 0.3 s. After injection the cells were allowed to recover for 30 min at 37°C in a 5% CO_2 atmosphere. At this point the cells were either prepared for live observation or fixed and prepared for immunofluorescence. Coverslips with live cells were mounted in a temperature-controlled cell chamber and observed by CLSM under a continuous flow of DMEM without the pH indicator phenol red and supplemented with 10% FCS and 20 mM HEPES–NaOH pH 7.4.

For immunofluorescence, the cells were fixed with 4% w/v paraformaldehyde in PBS for 10 min at room temperature, washed in PBS, quenched in 100 mM Tris–HCl pH 7.5, 50 mM NaCl for 5 min, permeabilized in 0.1% (v/v) Triton X-100 for 5 min and after washing with PBS incubated for 1 h with Cy5-labeled antibody in PBS containing 1% (w/v) BSA. After incubation, the cells were washed four times in PBS and mounted on glass slides using Mowiol 4.81 (Hoechst). All incubations were performed at room temperature. The antibodies used were anti-acyl-CoA oxidase (0.6 μg/ml) anti-bifunctional enzyme (0.3 μg/ml), anti-3-ketoacyl-CoA thiolase (0.3 μg/ml), anti-PMP70 (1.4 μg/ml) and anti-catalase (1.8 μg/ml). At these concentrations, the fluorescence signals were comparable.

Imaging techniques

Fluorescence images of cells were acquired on a confocal laser scanning microscope (CLSM; Zeiss LSM 310). Cy3 was excited with a 543 nm external He–Ne laser and detected using a 575 nm long-pass filter or, if incubated with Cy5-antibodies, using an Omega 590 ± 30 nm band pass filter. Cy5 was excited with a 633 nm He–Ne laser and detected using a 665 nm long-pass filter. The images were taken with a 40×1.3 NA oil immersion Plan-Neofluar objective.

FRET in donor-labeled cells was determined in a microscope by the combined acceptor and donor photobleaching methods (pbDIM) (Jovin and Arndt-Jovin, 1989; Gadella and Jovin, 1995; Bastiaens and Jovin, 1996, 1998; Bastiaens *et al*., 1996) according to the following sequence. (i) A pre-photobleach Cy3 (donor) image was acquired by scanning with 543 nm light in the CLSM. (ii) An intracellular region of interest (ROI) was selected and rendered free of Cy5 (acceptor) by repeated scanning with the 633 laser until all Cy5 was photodestructed. (iii) A second post-photobleach Cy3 image was acquired by scanning with a 543 nm laser. (iv) After correction for image registration (Bastiaens *et al*., 1996), the FRET efficiencies (E_i) in pixel *i* in the ROI were calculated from image arithmetic of the two (pre-photobleach, $I_{pre,i}$ and post-photobleach, $I_{post,i}$) Cy3 images.

$$E_i = \frac{I_{post,i} - I_{pre,i}}{I_{post,i}} \quad (1)$$

A second FRET determination in the complementary part of the ROI in the cells was performed by time-resolved donor photobleaching on a Zeiss Axioplan microscope equipped with a 100 W Hg lamp. The images were taken with a 40×1.3 NA oil immersion Plan-Neofluar objective. The fluorescent Cy3 label on the pre-nsL-TP was photobleached by excitation with 546 nm light (Zeiss 546BP12 bandpass filter) for 30 min. At 30 s intervals Cy3 fluorescence images were obtained by 10–25 s exposure with a cooled CCD camera (Photometrics Series 200) using FT580 dichroic (Zeiss) and SS600 Corion bandpass filters. Images were recorded until the signal was ~80% bleached and the sequence was fitted pixel-by-pixel to a single exponential decay and offset model by the program DECAY (Gadella and Jovin, 1995, 1997). The latter yielded the photobleaching time constant τ_i, amplitude a_i and offset c_i for each pixel *i*. FRET efficiencies for every pixel *i* (E_i) were then calculated from the ratio of photobleaching time (τ_i) and the average photobleaching time ($\langle\tau_r\rangle$) in the ROI in which Cy5 was photodestroyed:

$$E_i = 1 - \frac{\langle\tau_r\rangle}{\tau_i} \quad (2)$$

Statistical analyses averaged over the peroxisomal compartment of single cells were obtained by a sequence of image processing operations using IPLab (Signal Analytics), as follows. The local background contributions around the individual peroxisomes were estimated by applying a morphological filter to the confocal gray value data (erosion, i.e. minimum estimation, over a 5×5 neighborhood), and subtracting the result from the original images. A global threshold was used to generate binary masks for isolating the peroxisomes. The estimated parameters are defined and given in Table I.

Affinity chromatography

Pre-nsL-TP, lysozyme and BSA were dissolved in coupling buffer (100 mM Bicine–NaOH pH 8.3, 500 mM NaCl, 1 mM EDTA) at a concentration of 5 mg/ml. The protein solutions (1 ml) were added to CNBr-activated Sepharose 4B (0.7 ml) and allowed to react by incubation overnight at 4°C. Coupling efficiency exceeded 95% as estimated by protein determination. After coupling, the beads were incubated for 1 h at room temperature in 100 mM Tris–HCl pH 8.0, 1 mM EDTA to block the reactive groups and were washed by four cycles of 100 mM sodium

acetate pH 4.0, 1 mM EDTA and coupling buffer to remove unconjugated protein. The beads were loaded in glass columns (0.5×4 cm) and equilibrated in elution buffer (20 mM K-phosphate pH 6.4, 120 mM KCl, 1 mM EDTA). Non-specific protein binding sites were blocked by washing the affinity columns with 1 ml elution buffer containing 4 mg BSA.

The peroxisomal matrix fraction was transferred to elution buffer and concentrated to 0.4 mg/ml using an YM20 Centricon. Aliquots of these fractions (30 μg of protein) were applied to the column and 0.23 ml fractions were collected. Fractions were precipitated by trichloro-acetic acid, heated at 95°C for 5 min in sample buffer and subjected to SDS–polyacrylamide electrophoresis on 12.5% acrylamide gels according to Laemmli (1970).

Gels were electroblotted to nitrocellulose according to Kyhse-Andersen (1984) for 1 h at 1 mA/cm^2. After transfer, the nitrocellulose was stained for total protein with Coomassie Brilliant Blue. The blots were washed for 5 min with PBS and blocked in 2% (w/v) skimmed milk powder in PBS-Tween (PBS supplemented with 0.5% Tween-20) for 1 h. The blots were then incubated with primary antiserum diluted 1:2000 in 0.2% (w/v) non-fat dried milk powder in PBS-Tween for 1 h, washed three times for 10 min in 0.2% milk powder in PBS-Tween, incubated with GARPO diluted 1:15 000 in 0.2% milk powder in PBS-Tween for 1 h and washed three times for 10 min in 0.2% milk powder in PBS-Tween. Enhanced chemoluminescence (ECL) immunodetection was performed according to the protocol provided by Dupont NEN. Routinely, 5 min exposures were required to detect the specific protein.

Acknowledgements

We thank Teunis B.H.Geijtenbeek for providing purified recombinant pre-nsL-TP. This research was carried out under auspices of The Netherlands Foundation for Chemical Research (SON) and with financial aid from The Netherlands Organization for Scientific Research (NWO) and a grant from the Federation of European Biochemical Sciences (FEBS).

References

Antonenkov,V.D., Van Veldhoven,P.P., Waelkens,E. and Mannerts,G.P. (1997) Substrate specificities of 3-oxoacyl-CoA thiolase A and sterol carrier protein 2/3-oxoacyl-CoA thiolase purified from normal rat liver peroxisomes. Sterol carrier protein 2/3-oxoacyl-CoA thiolase is involved in the metabolism of 2-methyl-branched fatty acids and bile acid intermediates. *J. Biol. Chem.*, **272**, 26023–26031.

Baker,M.E., Billheimer,J.T. and Strauss,J.F.,III (1991) Similarity between the amino-terminal portion of mammalian 58-kD sterol carrier protein (SCPx) and *Escherichia coli* acetyl-CoA acyltransferase: evidence for a gene fusion in SCPx. *DNA Cell Biol.*, **10**, 695–698.

Bastiaens,P.I.H. and Jovin,T.M. (1996) Microspectroscopic imaging tracks the intracellular processing of a signal transduction protein: fluorescent-labeled protein kinase C β I. *Proc. Natl Acad. Sci. USA*, **93**, 8407–8412.

Bastiaens,P.I.H. and Jovin,T.M. (1998) Fluorescence resonance energy transfer microscopy. In Celis,J.E. (ed.), *Cell Biology: A Laboratory Handbook*. 2nd edn, Vol. 3. Academic Press, New York, NY, pp. 136–146.

Bastiaens,P.I.H., DeBeus,A., Lacker,M., Somerharju,P., Vauhkonen,M. and Eisinger,J. (1990) Resonance energy transfer from a cylindrical distribution of donors to a plane of acceptors. Location of apo-B100 protein on the human low-density lipoprotein particle. *Biophys. J.*, **58**, 665–675.

Bastiaens,P.I.H., Majoul,I.V., Verveer,P.J., Soeling,H.D. and Jovin,T.M. (1996) Imaging the intracellular trafficking and state of the AB5 quaternary structure of cholera toxin. *EMBO J.*, **15**, 4246–4253.

Billheimer,J.T. and Reinhart,M.P. (1990) Intracellular trafficking of sterols. *Subcell. Biochem.*, **16**, 301–331.

Billheimer,J.T., Strehl,L.L., Strauss,J.F.,III and Davis,L.G. (1990) Characterization of a cDNA encoding rat sterol carrier protein 2. *DNA Cell Biol.*, **9**, 159–165.

Bloj,B. and Zilversmit,D.B. (1977) Rat liver proteins capable of transferring phosphatidylethanolamine. Purification and transfer activity for other phospholipids and cholesterol. *J. Biol. Chem.*, **252**, 1613–1619.

Bloj,B. and Zilversmit,D.B. (1981) Accelerated transfer of neutral glycosphingolipids and ganglioside GM1 by a purified lipid transfer protein. *J. Biol. Chem.*, **256**, 5988–5991.

Bordier,C. (1981) Phase separation of integral membrane proteins in Triton X-114 solution. *J. Biol. Chem.*, **256**, 1604–1607.

Ceolotto,C., Flekl,W., Schorsch,F.J., Tahotna,D., Hapala,I., Hrastnik,C., Paltauf,F. and Daum,G. (1996) Characterization of a non-specific lipid transfer protein associated with the peroxisomal membrane of the yeast, *Saccharomyces cerevisiae. Biochim. Biophys. Acta*, **1285**, 71–78.

Chanderbhan,R., Noland,B.J., Scallen,T.J. and Vahouny,G.V. (1982) Sterol carrier protein-2. Delivery of cholesterol from adrenal lipid droplets to mitochondria for pregnenolone synthesis. *J. Biol. Chem.*, **257**, 8928–8934.

Crain,R.C. and Zilversmit,D.B. (1980) Two nonspecific phospholipid exchange proteins from beef liver. I. Purification and characterization. *Biochemistry*, **19**, 1433–1439.

Frolov,A., Cho,T.H., Billheimer,J.T. and Schroeder,F. (1996) Sterol carrier protein-2, a new fatty acyl coenzyme A-binding protein. *J. Biol. Chem.*, **271**, 31878–31884.

Fujiki,Y., Tsuneoka,M. and Tashiro,Y. (1989) Biosynthesis of nonspecific lipid transfer protein (sterol carrier protein 2) on free polyribosomes as a larger precursor in rat liver. *J. Biochem.*, **106**, 1126–1131.

Gadella,T.W.J.,Jr and Jovin,T.M. (1995) Oligomerization of epidermal growth factor receptors on A431 cells studied by time-resolved fluorescence imaging microscopy. A. stereochemical model for tyrosine kinase receptor activation. *J. Cell Biol.*, **129**, 1543–1558.

Gadella,T.W.J.,Jr and Jovin,T.M. (1997) Fast algorithms for the analysis of single and double exponential decay curves with a background term. Application to time-resolved imaging microscopy. *Bioimaging*, **5**, 5–39.

Gadella,T.W.J.,Jr and Wirtz,K.W.A. (1991) The low-affinity lipid binding site of the non-specific lipid transfer protein. Implications for its mode of action. *Biochim. Biophys. Acta*, **1070**, 237–245.

Geelen,M.J.H., Beynen,A.C. and Wirtz,K.W.A. (1987) Cholesterol metabolism and sterol carrier protein-2 (non-specific lipid transfer protein). *Int. J. Biochem.*, **19**, 619–623.

Gould,S.J., Keller,G.A. and Subramani,S. (1987) Identification of a peroxisomal targeting signal at the carboxy terminus of firefly luciferase. *J. Cell Biol.*, **105**, 2923–2931.

Gould,S.J., Keller,G.A., Hosken,N., Wilkinson,J. and Subramani,S. (1989) A conserved tripeptide sorts proteins to peroxisomes. *J. Cell Biol.*, **108**, 1657–1664.

Gould,S.J., Keller,G.A., Schneider,M., Howell,S.H., Garrard,L.J., Goodman,J.M., Distel,B., Tabak,H.F. and Subramani,S. (1990) Peroxisomal protein import is conserved between yeast, plants, insects and mammals. *EMBO J.*, **9**, 85–90.

Johnson,W.J. and Reinhart,M.P. (1994) Lack of requirement for sterol carrier protein-2 in the intracellular trafficking of lysosomal cholesterol. *J. Lipid Res.*, **35**, 563–573.

Jovin,T.M. and Arndt-Jovin,D.J. (1989) FRET microscopy: digital imaging of fluorescence resonance energy transfer. Application in cell biology. In Kohen,E., Ploem,J.S. and Hirschberg,J.G. (eds), *Cell Structure and Function by Microspectrofluorometry*. Academic Press, Orlando, FL, pp. 99–117.

Keller,G.A., Scallen,T.J., Clarke,D., Maher,P.A., Krisans,S.K. and Singer,S.J. (1989) Subcellular localization of sterol carrier protein-2 in rat hepatocytes: its primary localization to peroxisomes. *J. Cell Biol.*, **108**, 1353–1361.

Kyhse-Andersen,J. (1984) Electroblotting of multiple gels: a simple apparatus without buffer tank for rapid transfer of proteins from polyacrylamide to nitrocellulose. *J. Biochem. Biophys. Methods*, **10**, 203–209.

Laemmli,U.K. (1970) Cleavage of structural proteins during the assembly of the head of bacteriophage T4. *Nature*, **227**, 680–685.

Litwin,J.A. and Bilinska,B. (1995) Morphological heterogeneity of peroxisomes in cultured mouse Leydig cells. *Folia Histochem. Cytobiol.*, **33**, 255–258.

Moncecchi,D., Pastuszyn,A. and Scallen,T.J. (1991) cDNA sequence and bacterial expression of mouse liver sterol carrier protein-2. *J. Biol. Chem.*, **266**, 9885–9892.

Niki,T., Bun-Ya,M., Hiraga,Y., Muro,Y. and Kamiryo,T. (1994) Near-stoichiometric interaction between the non-specific lipid-transfer protein of the yeast *Candida tropicalis* and peroxisomal acyl-coenzyme A oxidase prevents the thermal denaturation of the enzyme *in vitro*. *Yeast*, **10**, 1467–1476.

Ossendorp,B.C., Van Heusden,G.P.H., De Beer,A.L.J., Bos,K., Schouten,G.L. and Wirtz,K.W.A. (1991) Identification of the cDNA clone which encodes the 58-kDa protein containing the amino acid sequence of rat liver non-specific lipid-transfer protein (sterol-carrier

protein 2). Homology with rat peroxisomal and mitochondrial 3-oxoacyl-CoA thiolases. *Eur. J. Biochem.*, **201**, 233–239.
Ossendorp,B.C., Geijtenbeek,T.B.H. and Wirtz,K.W.A. (1992) The precursor form of the rat liver non-specific lipid-transfer protein, expressed in *Escherichia coli*, has lipid transfer activity. *FEBS Lett.*, **296**, 179–183.
Ossendorp,B.C., Snoek,G.T. and Wirtz,K.W.A. (1994) Intracellular phospholipid transfer proteins. *Curr. Topics Membr.*, **40**, 217–259.
Osumi,T., Hashimoto,T. and Ui,N. (1980) Purification and properties of acyl-CoA oxidase from rat liver. *J. Biochem.*, **87**, 1735–1746.
Phizicky,E.M. and Fields,S. (1995) Protein–protein interactions: methods for detection and analysis. *Microbiol. Rev.*, **59**, 94–123.
Schrader,M., Baumgart,E., Völkl,A. and Fahimi,H.D. (1994) Heterogeneity of peroxisomes in human hepatoblastoma cell line HepG2. Evidence of distinct subpopulations. *Eur. J. Cell Biol.*, **64**, 281–294.
Schrader,M., Baumgart,E. and Fahimi,H.D. (1995) Effects of fixation on the preservation of peroxisomal structures for immunofluorescence studies using HepG2 cells as a model system. *Histochem. J.*, **27**, 615–619.
Schrader,M., Burkhardt,J.K., Baumgart,E., Lüers,G., Spring,H., Völkl,A. and Fahimi,H.D. (1996) Interaction of microtubules with peroxisomes. Tubular and spherical peroxisomes in HepG2 cells and their alterations induced by microtubule-active drugs. *Eur. J. Cell Biol.*, **69**, 24–35.
Seedorf,U. and Assmann,G. (1991) Cloning, expression and nucleotide sequence of rat liver sterol carrier protein 2 cDNAs. *J. Biol. Chem.*, **266**, 630–636.
Seedorf,U., Brysch,P., Engel,T., Schrage,K. and Assmann,G. (1994) Sterol carrier protein X is peroxisomal 3-oxoacyl coenzyme A thiolase with intrinsic sterol carrier and lipid transfer activity. *J. Biol. Chem.*, **269**, 21277–21283.
Seedorf,U. *et al*. (1998) Defective peroxisomal catabolism of branched fatty acyl coenzyme A in mice lacking the sterol carrier protein-2/ sterol carrier protein-X gene function. *Genes Dev.*, **12**, 1189–1201.
Southwick,P.L., Ernst,L.A., Tauriello,E.W., Parker,S.R., Mujumdar,R.B., Mujumdar,S.R., Clever,H.A. and Waggoner,A.S. (1990) Cyanine dye labeling reagents—carboxymethylindocyanine succinimidyl esters. *Cytometry*, **11**, 418–430.
Subramani,S. (1998) Components involved in peroxisome import, biogenesis, proliferation, turnover and movement. *Physiol. Rev.*, **78**, 171–188.
Suzuki,Y., Yamaguchi,S., Orii,T., Tsuneoka,M. and Tashiro,Y. (1990) Nonspecific lipid transfer protein (sterol carrier protein-2) defective in patients with deficient peroxisomes. *Cell Struct. Funct.*, **15**, 301–308.
Tan,H., Bun-ya,M., Hirata,A. and Kamiryo,T. (1994) Predominant localization of non-specific lipid-transfer protein of the yeast *Candida tropicalis* in the matrix of peroxisomes. *Yeast*, **10**, 1065–1074.
Trzeciak,W.H., Simpson,E.R., Scallen,T.J., Vahouny,G.V. and Waterman, M.R. (1987) Studies on the synthesis of sterol carrier protein-2 in rat adrenocortical cells in monolayer culture. Regulation by ACTH and dibutyryl cyclic 3′,5′-AMP. *J. Biol. Chem.*, **262**, 3713–3717.
Tsuneoka,M., Yamamoto,A., Fujiki,Y. and Tashiro,Y. (1988) Nonspecific lipid transfer protein (sterol carrier protein-2) is located in rat liver peroxisomes. *J. Biochem. (Tokyo)*, **104**, 560–564.
Van der Krift,T.P., Leunissen,J., Teerlink,T., Van Heusden,G.P.H., Verkleij,A.J. and Wirtz,K.W.A. (1985) Ultrastructural localization of a peroxisomal protein in rat liver using the specific antibody against the non-specific lipid transfer protein (sterol carrier protein 2). *Biochim. Biophys. Acta*, **812**, 387–392.
Van Haren,L., Teerds,K.J., Ossendorp,B.C., Van Heusden,G.P.H., Orly,J., Stocco,D.M., Wirtz,K.W.A. and Rommerts,F.G. (1992) Sterol carrier protein 2 (non-specific lipid transfer protein) is localized in membranous fractions of Leydig cells and Sertoli cells but not in germ cells. *Biochim. Biophys. Acta*, **1124**, 288–296.
Van Heusden,G.P.H., Souren,J., Geelen,M.J.H. and Wirtz,K.W.A. (1985) The synthesis and esterification of cholesterol by hepatocytes and H35 hepatoma cells are independent of the level of nonspecific lipid transfer protein. *Biochim. Biophys. Acta*, **846**, 21–25.
Van Heusden,G.P.H., Bos,K. and Wirtz,K.W.A. (1990) The occurrence of soluble and membrane-bound non-specific lipid transfer protein (sterol carrier protein 2) in rat tissues. *Biochim. Biophys. Acta*, **1046**, 315–321.
Van Heusden,G.P.H., Van Beckhoven,J.C.R.M., Thieringer,R., Raetz,C.R.H. and Wirtz,K.W.A. (1992) Increased cholesterol synthesis in Chinese hamster ovary cells deficient in peroxisomes. *Biochim. Biophys. Acta*, **1126**, 81–87.
Völkl,A. and Fahimi,H.D. (1985) Isolation and characterization of peroxisomes from the liver of normal untreated rats. *Eur. J. Biochem.*, **149**, 257–265.
Walton,P.A., Gould,S.J., Feramisco,J.R. and Subramani,S. (1992) Transport of microinjected proteins into peroxisomes of mammalian cells: inability of Zellweger cell lines to import proteins with the SKL tripeptide peroxisomal targeting signal. *Mol. Cell. Biol.*, **12**, 531–541.
Wanders,R.J.A., Denis,S., Wouters,F.S., Wirtz,K.W.A. and Seedorf,U. (1997) Sterol carrier protein X (SCPx) is a peroxisomal branched-chain β-ketothiolase specifically reacting with 3-oxo-pristanoyl-CoA: a new, unique role for SCPx in branched-chain fatty acid metabolism in peroxisomes. *Biochem. Biophys. Res. Commun.*, **236**, 565–567.
Wilcke,M., Hultenby,K. and Alexson,S.E. (1995) Novel peroxisomal populations in subcellular fractions from rat liver. Implications for peroxisome structure and biogenesis. *J. Biol. Chem.*, **270**, 6949–6958.
Wouters,F.S. (1997) nsL-TP and peroxisomal β-oxidation. PhD thesis. University of Utrecht, Utrecht, The Netherlands.
Yamamoto,K. and Fahimi,H.D. (1987) Three-dimensional reconstruction of a peroxisomal reticulum in regenerating rat liver: evidence of interconnections between heterogeneous segments. *J. Cell Biol.*, **105**, 713–722.

Received May 13, 1998; revised August 27, 1998; accepted October 12, 1998